Naval Surface Warfare Center
Carderock Division
West Bethesda, MD 20817-5700

NSWCCD-61-TR–2003/09 September 2003

Survivability, Structures, and Materials Directorate

Technical Report

Spray Forming Iron Based Amorphous Metals

by

Leslie K. Kohler

Louis F. Aprigliano

A. Srinivasa Rao

NSWCCD-61-TR–2003/09 Spray Forming Iron Based Amorphous Metals

Naval Surface Warfare Center
Carderock Division
West Bethesda, MD 20817-5700

NSWCCD-61-TR–2003/09 September 2003

Survivability, Structures, and Materials Directorate
Technical Report

Spray Forming Iron Based Amorphous Metals

by
Leslie K. Kohler
Louis F. Aprigliano
A. Srinivasa Rao

REPORT DOCUMENTATION PAGE

Form Approved OMB No. 0704-0188

1. AGENCY USE ONLY (Leave blank)	2. REPORT DATE	3. REPORT TYPE AND DATES COVERED
	September 2003	Research and Development

4. TITLE AND SUBTITLE
Spray Forming Iron Based Amorphous Metals

5. FUNDING NUMBERS

6. AUTHOR(S)
Leslie K. Kohler
Louis F. Aprigliano
A. Srinivasa Rao

7. PERFORMING ORGANIZATION NAME(S) AND ADDRESS(ES)
Naval Surface Warfare Center, Carderock Division
Code 612, Metals Processing and Analysis Branch
West Bethesda, Maryland 20817

8. PERFORMING ORGANIZATION REPORT NUMBER
NSWCCD 61-TR-2003/09

9. SPONSORING/MONITORING AGENCY NAME(S) AND ADDRESS(ES)
Defense Advanced Research Projects Agency
Defense Science Office
Dr. Leo Christodoulou
3701 North Fairfax Dr.
Arlington, VA 22203-1714

10. SPONSORING/MONITORING AGENCY REPORT NUMBER

11. SUPPLEMENTARY NOTES

12a. DISTRIBUTION/AVAILABILITY STATEMENT
Distribution unlimited. Approved for public release.

12b. DISTRIBUTION CODE

13. ABSTRACT (Maximum 200 words)

Spray metal forming has been used to produce deposits of iron-based alloys DAR1A, DAR 27, DAR35, and BMA1. The deposits were made on tubular and flat plate substrates and were up to 1.25 inches in thickness. Most of the deposits were found to be partially amorphous in the as-sprayed condition. Measurements were made of microhardness and porosity, and corrosion and wear tests were conducted. Severe cracking occurred in the thick section spray formed deposits, most likely arising from thermal stresses. The use of a pre-heated substrate is being investigated to minimize or eliminate this cracking. The spray formed deposits had high hardness (900 to 1200 HV), low porosity, (0.5 to 3%), and better wear resistance than a conventional hull steel and a tool steel. In a standardized salt fog chamber test, the spray formed alloys were found to corrode like conventional hull steel. This is probably a result of the partially devitrified nature of the spray formed material.

14. SUBJECT TERMS
Structural Amorphous Metals, SAMs, Spray Metal Forming, Amorphous Metals

15. NUMBER OF PAGES
46

16. PRICE CODE

17. SECURITY CLASSIFICATION OF REPORT	18. SECURITY CLASSIFICATION OF THIS PAGE	19. SECURITY CLASSIFICATION OF ABSTRACT	20. LIMITATION OF ABSTRACT
UNCLASSIFIED	UNCLASSIFIED	UNCLASSIFIED	UNCLASSIFIED

Contents

	Page
Abstract	v
Administrative Information	v
Acknowledgements	v
Introduction	1
Experimental Procedure	2
Materials	2
Chemistries	2
Spray Forming Runs	2
Hardness and Porosity Measurements	3
X-ray Diffraction Parameters	4
Differential Scanning Calorimetry (DSC) and Differential Thermal Analysis (DTA)	4
Corrosion Tests	5
Wear Tests	5
Results and Discussion	6
Chemistries	6
Cracking	8
Hardness	8
Porosity	9
Amorphous Phase Detection	10
Macroscopy	13
Microscopy	15
Corrosion Results	19
Wear Test Results	22
Summary	23
References	25
Appendix A. Abrasive Wear Tests of Various Coupons	A-1

Figures

		Page
Figure 1.	Spray Metal Forming Process	1
Figure 2.	ASTM G-65 Wear Test Setup	6
Figure 3.	Example of a Wear Scar	6
Figure 4.	Tubular Run 523 - DAR1A	8
Figure 5.	Flat Plate Run 532 - DAR27	8
Figure 6.	Microhardness Indentations	9
Figure 7.	Run 523 Fracture Surface - DAR1A	10
Figure 8.	Run 527 Fracture Surface - DAR27	10
Figure 9.	DSC plots of DAR1A and DAR27 Alloys in Spray Formed, Ingot, and Powder Forms	11
Figure 10.	XRD Patterns for Samples From Spray Forming Runs 523 and 524	11
Figure 11.	XRD of Material From Beginning Section of Run 536	12
Figure 12.	XRD of Material From End Section of Run 536	12

Figures (continued)

Figure 13. XRD Patterns For Run 537, DAR35 13
Figure 14. DAR 1A, Run 523, Mag. 2x 13
Figure 15. Optical Macrographs of Fracture Surface on Piece of As-sprayed DAR35 From Run 537 14
Figure 16. Scanning Electron Microscope, Secondary Electron Image of Fracture Surface on Piece of As-sprayed DAR35 From Run 537 14
Figure 17. Optical Microscope Image of DAR35, Run 537, Etched 15
Figure 18. Scanning Electron Microscope, Backscattered Electron Image, DAR35, Run 537, Unetched 16
Figure 19. Optical microscope image of DAR27, Run 532, etched 17
Figure 20. Scanning Electron Microscope, Backscattered Electron Image, DAR27, Run 532, Unetched 18
Figure 21. Photographs of Salt Fog Corrosion Samples of DAR1A, Run 535 Before and After Exposure 20
Figure 22. Photographs of Salt Fog Corrosion Samples of DAR27, Run 532 Before and After Exposure 20
Figure 23. Photographs of Salt Fog Corrosion Samples of DAR35 (Run 537), DAR1A (Run 536), HSLA 80 and Inconel 625 after 5 cycles 21

Tables

		Page
Table 1.	Iron Based Amorphous Metal Compositions in Atomic Percent	2
Table 2.	Spray Forming Run Details	3
Table 3.	24 Hour Test Cycle for GM9540P Accelerated Corrosion Test	5
Table 4.	Chemical Analysis of Spray Formed Samples Compared to Nominal Compositions in Atomic Percent and for Oxygen and Nitrogen Also in Weight Percent (wt. %)	7
Table 5.	Microindentation Hardness (Vickers) Results	9
Table 6.	Phase Equivalences Between Optical (Figure 17) and BSE (Figure 18) Images of DAR35, Run 537	16
Table 7.	Comparison of Specimen Wear Rates	22

Abstract

Spray metal forming has been used to produce deposits of iron-based alloys DAR1A, DAR 27, DAR35, and BMA1. The deposits were made on tubular and flat plate substrates and were up to 1.25 inches in thickness. Most of the deposits were found to be partially amorphous in the as-sprayed condition. Measurements were made of microhardness and porosity, and corrosion and wear tests were conducted. Severe cracking occurred in the thick section spray formed deposits, most likely arising from thermal stresses. The use of a pre-heated substrate is being investigated to minimize or eliminate this cracking. The spray formed deposits had high hardness (900 to 1200 HV), low porosity, (0.5 to 3%), and better wear resistance than a conventional hull steel and a tool steel. In a standardized salt fog chamber test, the spray formed alloys were found to corrode like a conventional hull steel. This is probably a result of the partially devitrified nature of the spray formed material.

Administrative Information

The work described in this report was performed by the Metals Department (Code 61) of the Survivability, Structures and Materials Directorate at the Naval Surface Warfare Center, Carderock Division (NSWCCD). The work was funded by the Defense Advanced Research Projects Agency, DARPA, and administered by Dr. Leo Christodoulou. This work was performed at the NSWCCD under the contract number: W08041-10 and work unit number 02-1-6120-510. This work was supervised by Dr. L. F. Aprigliano of Code 612.

Acknowledgements

The authors would like to thank Dr. Daniel Branagan, formerly of the Idaho National Engineering and Environmental Laboratory (INEEL) and Dr. Joe Poon of the University of Virginia, for providing compositions and materials and George Wolter of HOWMET for his chemistry check and metallography of a spray run sample. The authors also acknowledge the use of x-ray diffraction facilities at the George Washington University which was funded by a grant from the National Science Foundation. NSWCCD colleagues performing experimental work included Robert Mattox for spray forming, Steven Dallek for thermal analysis, Denise Aylor for corrosion testing and Albert Brandemarte, Richard Stockhausen and Karen Witkoski for microscopy.

This page intentionally left blank

Introduction

Amorphous metals – those without long-range atomic order – are novel materials that have the potential for unique properties.[1] Historically, their research and production has been limited to very thin products or coatings due to the inherently high critical cooling rates (>10^6K/s) needed to inhibit crystallization and the absence of suitable rapid solidification techniques. Recent advances in alloy development have produced new compositions with reduced critical cooling rates of less than 10^3 K/s. Cooling rates of this magnitude can be achieved through spray processes such as metal spray forming, high velocity oxy fuel (HVOF) thermal spray, and wire arc spray.

Metal spray forming is of particular interest because it is a bulk forming process, whereas thermal spray techniques such as HVOF and wire arc are used for coatings. Metal spray forming, shown in Figure 1, is a single process consisting of 3 stages: melting, atomization, and deposition. Rapid solidification occurs within the spray, where droplets experience cooling on the order of 10^3-10^4 K/s. The atomization and deposition occurs at a rate of 25 - 60 lb/min. The substrate can be many different shapes, and is manipulated beneath the spray in order to obtain as uniform of a deposit as possible. Examples of a tube, a plate, and a billet are shown in Figure 1.

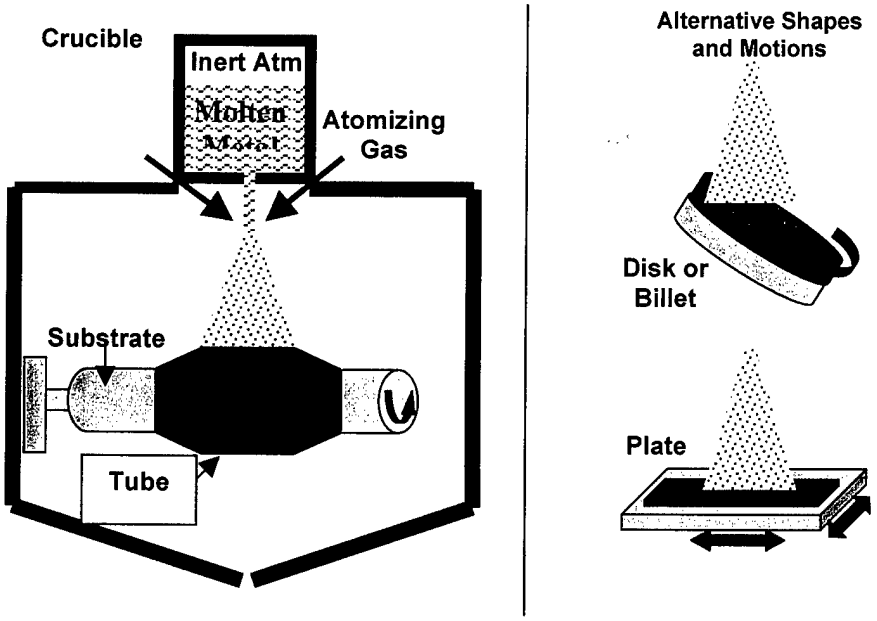

a. Process schematic

b. Alternative shapes and motions

Figure 1. Spray Metal Forming Process.

The objective of this study was to evaluate metal spray forming as a processing technique for iron-based amorphous alloys and to evaluate individual compositions for their physical properties and ability to form an amorphous microstructure.

Experimental Procedure

Materials

The four compositions included in this report are listed in Table 1. The first three compositions were invented and provided by Daniel Branagan, formerly of INEEL and now of The Nanosteel Company. The fourth composition is one that is taken from literature and is reported[2] to have the lowest known critical cooling rate (10K/s) for an iron based amorphous alloy to date. These iron based compositions are sometimes referred to as structural amorphous metals (SAMs).

Table 2. Iron Based Amorphous Metal Compositions in Atomic Percent.

	Fe	Cr	Mo	C	B	Si	W	Mn	Al	Ga	P
DAR1A	63	8	2	5	17	1	-	-	4	-	-
DAR27	58.4	14.6	2	4	16	1	2	2	-	-	-
DAR35	54.5	15	2	4	16	5	1.5	2	-	-	-
BMA1	72	-	-	6	4	1	-	-	5	2	10

Chemistries

The chemistries of the alloys were checked in some of the finished spray metal formed products. This work was done by a commercial vendor. The nitrogen and oxygen contents were determined by inert gas fusion (IGF). The carbon was determined by high temperature combustion (COMB). The other elements were done by inductively coupled plasma, optical emission (ICP-OE).

Spray Forming Runs

Seven experimental spray forming runs with DAR1A have been completed, five of which used a tubular substrate of 6" outer diameter. The other two runs of DAR1A were sprayed onto a flat copper plate in an attempt to produce sheet material. Four of the tubular substrates were thin walled mild steel, and one was a thick walled titanium substrate. The titanium substrate was expected to provide better thermal conductivity and more thermal mass in order to contribute to cooling in the deposit, but more experimental runs would be needed in order to truly evaluate this effect. In addition to the DAR1A runs, three successful runs were made with DAR27 on substrates of stainless steel plate or tube; one run was made with BMA1 on a copper plate substrate; and one run was made with DAR35 on a titanium plate substrate.

Spray forming Run 537 (DAR35) was an attempt to make a flat plate by spraying on a titanium substrate. Previous runs that were sprayed onto copper plates with DAR27 showed a tendency of the sprayed material to react along its perimeter with the copper plate. This reaction

zone constrained the sprayed material from freely contracting upon cooling. This is believed to have exacerbated the cracking of the sprayed material to be discussed below. The titanium was used in Run 537, since previous test have shown that other iron-based alloys did not react with titanium substrates.

Selected details of each of the runs to date are shown in Table 2. In order to maximize cooling rate, high gas flow and low metal flow rates were used in the runs. These parameters combine to form the benchmark gas to metal ratio (GMR). Since higher than normal gas flow rates and pressures are being used, some process failures occurred as noted for Runs 525, 528, and 533. Additional process failures occurred while attempting to spray form billet shapes (runs 529 and 530). In general, billets require even higher GMR values than for tubes or plates, and this requirement was not achieved with the current laboratory setup. All of the runs were made in our non-reactive spray facility with a 50 pound crucible melt system. Nitrogen was used as the melt cover gas and as the atomization gas.

Table 2. Spray Forming Run Details.

Run #	Composition	Substrate	GMR	Comments
523	DAR1A	6" Dia. Tube	4.49	
524	DAR1A	6" Dia. Ti Tube	2.77	
525	DAR1A	Tube	N/A	freeze off
526	DAR1A	Tube	6.47	
527	DAR27	Tube	2.42	
528	DAR27	Billet	N/A	freeze off
529	DAR27	Billet	N/A	crucible broke
530	DAR27	Billet	N/A	too hot
531	DAR27	SS plate	2.09	
532	DAR27	SS plate	2.18	
533	DAR27	Cu plate	N/A	freeze off
534	DAR1A	Cu plate	3.12	
535	DAR1A	Cu plate	1.95	
536	BMA1	Cu plate	1.82	
537	DAR35	Ti plate	2.21	

Hardness and Porosity Measurements

Vickers hardness measurements were made at two loads, 1000g and 100g. Readings were made with a sample from one of the tubular runs, Run 523 (DAR1A) and seven of the flat plate runs, Runs 531 (DAR27), 532 (DAR27), 534 (DAR1A), 535 (DAR1A), 536 (BMA), and 537 (DAR35). In the case of the samples from the flat plate runs, readings were taken near the top, the middle, and the bottom (the part closest to the substrate) of the samples cross-sections.

Porosity readings were made using a CLEMEX™ image analyzer.

X-Ray Diffraction Parameters

To check for the presence of crystalline material, a Sintag XDS-2000 x-ray diffractometer with a $CuK_{\alpha}1$ source at 8048 eV, -2.5 FWHM was used during this investigation. The x-ray source energy, and the applied current values were 40KV, and - 40 mA, respectively. Most of the SAM samples that were analyzed were typically 2 cm x 1 cm x 0.5 cm (thickness). However, a few larger samples [2 cm x 2 cm x 3 cm (thickness)] were also studied with the x-ray diffractometer.

During this investigation, it was found that when all the filters [2 on the x-ray source side (slit size 4 and 2 mm) and 2 on the detector side (slit size 0.5 and 0.2 mm)] were positioned, the output signal was very weak and no meaningful x-ray diffraction (XRD) was obtained. By trial and error, we found that good output signal can be obtained when the fine filter (slit size 0.2 mm) on the collector side is removed. Therefore, during the present investigation, all the x ray diffraction patterns were obtained with only three filters (4 mm and 2 mm on the x-ray source side and only 0.5 mm filter on the detector side). The diffraction patterns were obtained under continuous 2 theta scan mode. The scans were made over the 2 theta value of 10 – 90 degrees. During the scan, the sample with respect to the detector also rotates and the rotation (called omega) is always half that of the 2 theta. Therefore the omega values that correspond to the 2 theta values of 10 – 90 degrees were 5 and 45 degrees respectively. The total time for each measurement was approximately 3 hours. Each sample was first measured at a faster scan rate of 1 degree per minute. Once the quick scan indicates a good x ray diffraction pattern, the final measurement was made at a slower scan rate of 1 degree per 3 minutes.

Differential Scanning Calorimetry (DSC) and Differential Thermal Analysis (DTA)

Differential scanning calorimetry (DSC) is: "A technique for measuring the temperature, direction, and magnitude of thermal transitions in a sample material by heating/cooling and comparing the amount of energy required to maintain its rate of temperature increase or decrease with an inert reference material under similar conditions."[3] If a material contains a glassy phase that crystallizes upon heating it will show up as a spike in the DSC plots. DSC experiments were conducted with a TA Instruments 2920 differential scanning calorimeter. Samples were encapsulated in aluminum pans and heated at a rate of 20 K/min from 298 to 898 K. The DSC cell was purged with nitrogen at a rate of 70 cm^3/min.

Differential thermal analysis (DTA) is: "A technique for observing the temperature, direction, and magnitude of thermally induced transitions in a material by heating/cooling a sample and comparing its temperature with that of an inert reference material under similar conditions."[3] If a material contains a glassy phase that re-crystallizes upon heating it will show up as a spike in the DTA plots. In our thermal analysis laboratory at NSWCCD, DTA is used when it is suspected that crystallization will occur at a temperature above 898 K. DTA experiments were conducted with a TA Instruments 2960 TGA-DTA. Samples were heated in alumina pans at a rate of 20 K/min from 298 to 1223 K. The instrument was purged with nitrogen at a rate of 100 cm^3/min.

Corrosion Tests

Samples from Runs 532 (DAR27), 535 (DAR1A), 536 (BMA), and 537 (DAR27) were exposed to a salt fog corrosion test. The details of the 24 hour test cycle used are given below in Table 3.

Table 3. 24 Hour Test Cycle for GM9540P Accelerated Corrosion Test.

Shift	*Elapsed Time (hrs)*	*Event*
Ambient Soak	0	*Salt solution mist for 30 seconds, followed by ambient exposure (13-28 °C (55-82 °F))
	1.5	*Salt solution mist for 30 seconds, followed by ambient exposure (13-28 °C (55-82 °F))
	3	*Salt solution mist for 30 seconds, followed by ambient exposure (13-28 °C (55-82 °F))
	4.5	*Salt solution mist for 30 seconds, followed by ambient exposure (13-28 °C (55-82 °F))
Wet Soak	8-16	8 hour high humidity exposure (49 ± 0.5 °C (120 ± 1 °F), 100% RH) including 55 minute ramp to wet conditions
Dry Soak	16-24	8 hour elevated dry exposure (60 ± 0.5 °C (140 ± 1 °F), <30% RH) including 175 minute ramp to dry conditions

*Salt solution mist consists of 1.25% solution containing 0.9% sodium chloride, 0.1% calcium chloride, and 0.25% sodium bicarbonate.

Wear Tests

Samples from selected runs of spray metal formed material were subjected to a standardized (ASTM G-65) dry sand wear test. The samples were from Runs 531 (DAR27), 536 (BMA), and 537 (DAR27). Samples of a typical naval hull steel, HSLA 100, and a tool steel, D2 Tool Steel, were also tested for comparison purposes. The wear test method used is schematically represented in Figure 2. A typical wear scar is shown in Figure 3. The wear testing was performed at Colorado State University (CSU). Wear resistance was measured as a function of mass loss. These measurements were then converted to volume loss values based on material densities of the coatings. Further details on the wear test procedure can be found in Appendix A.

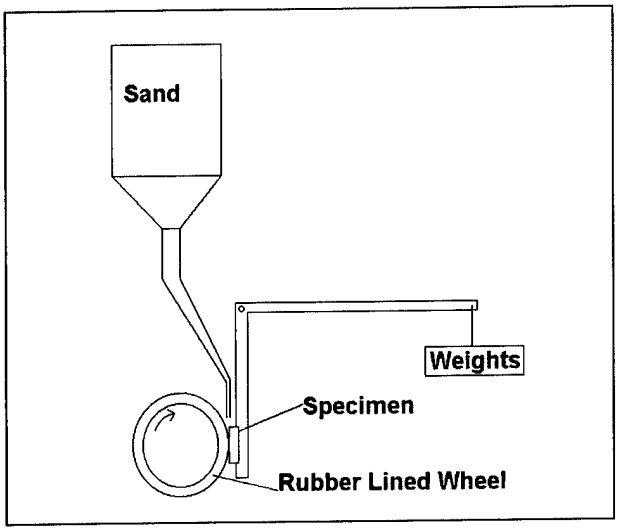

Figure 2. ASTM G-65 Wear Test Setup.

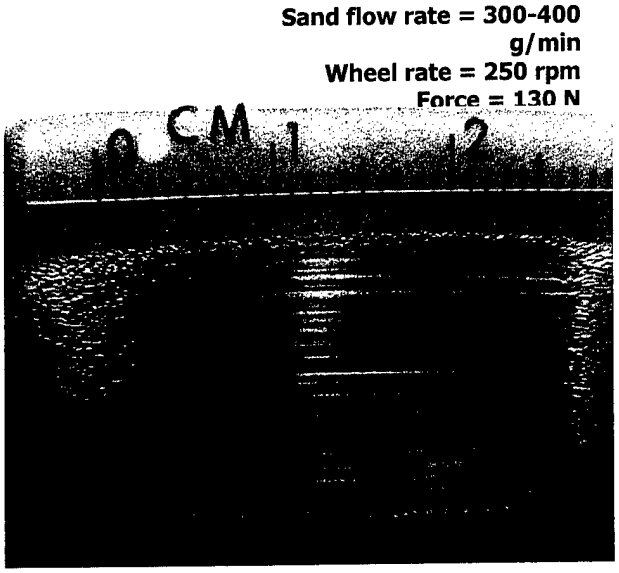

Figure 3. Example of a Wear Scar.

Results and Discussion

Chemistries

The chemistries of the starting materials and selected spray runs are given in Table 4. The as-sprayed chemistries were all near the starting ingot/material nominal values. The oxygen and nitrogen content of the spray formed materials was low. In the case of DAR27 the low values were confirmed in independent testing by George Wolter of HOWMET. The HOWMET results showed 33 ppm oxygen and 99 ppm nitrogen for spray formed DAR27.

Table 4. Chemical Analysis of Spray Formed Samples Compared to Nominal Compositions in Atomic Percent and for Oxygen and Nitrogen Also in Weight Percent (wt. %).

	Fe	Cr	Mo	C	B	Si	W	Mn	Al	Ga	P	O (wt. %)	N (wt. %)
DAR1A Nominal	63	8	2	5	17	1	-	-	4	-	-		
DAR1A Spray Formed #535	60.1	7.7	2.0	4.6	20.1	0.9	-	0.02	4.5	-	-	0.015 (0.0056)	0.005 (0.0017)
DAR27 Nominal	58.4	14.6	2	4	16	1	2	2	-	-	-		
DAR27 Spray Formed #532	56.8	14.2	1.8	3.9	17.9	1.3	1.9	1.9	-	-	-	0.010 (0.0033)	0.037 (0.0108)
DAR35 Nominal	54.5	15	2	4	16	5	1.5	2	-	-	-		
DAR35 Spray Formed #537	53.7	15	1.87	4.2	15.8	5.7	1.3	2.2				0.02 (0.0069)	0.02 (0.0070)
BMA1 Nominal	72	-	-	6	4	1	-	-	5	2	10		
BMA1 Spray Formed #536	70.2	-	-	5.8	4.6	1.2	-	0.3	4.5	2	10.8	0.013 (0.0045)	<0.0001 (<0.0003)

Cracking

All of the spray formed deposits to date have had severe cracking during the slow cooling phase of the process. In the case of the tubular substrates, this has caused material to fall off of the substrate after spray forming is complete. Examples of cracking in the tubular and flat plate runs are shown in Figures 4 and 5 below. Possible causes for these cracks and spalling are thermal mismatch at the substrate/deposit interface and/or thermal stresses built up within the deposit due to rapid cooling. It is also noted that these alloy compositions are particularly brittle in their ingot form as well - all ingots received to be melted from INEEL were broken into several pieces and could be easily fractured on impact with a conventional hammer.

In Run 537 a titanium substrate was used in an effort to minimize cracking. Run 537 had less cracking than previous runs, but still cracked.

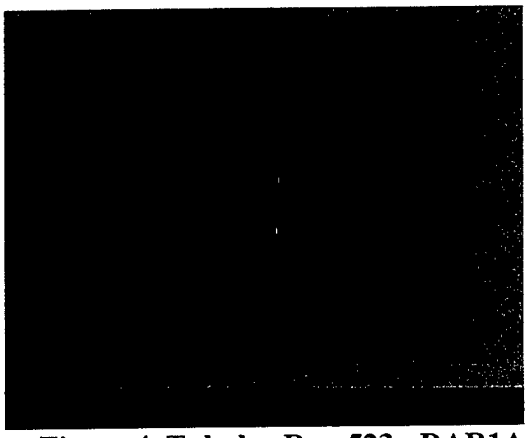

Figure 4. Tubular Run 523 - DAR1A

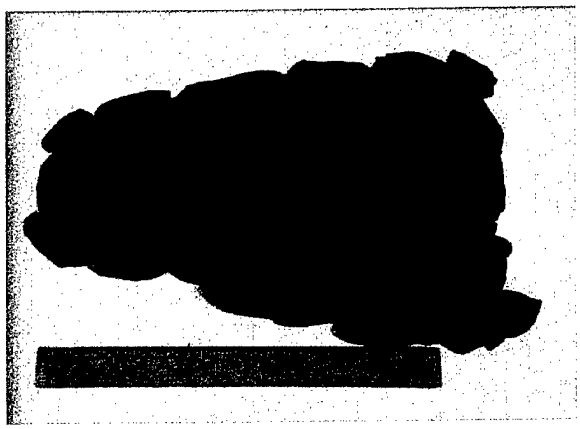

Figure 5. Flat Plate Run 532 - DAR27

Hardness

The microhardness results for material from the flat plate runs are given in Table 5. The majority of the microhardness indentations made in material from runs of alloys DAR1A, BMA, and DAR 27 produced cracks at the corners of the diamond shaped impressions. Figure 6a is an example of this cracking. The only material in which the majority of the microhardness indentations did not produce cracking was Run 537, DAR35. Furthermore, there are even some signs of plasticity along the edges of the diamond shaped indentations (Figure 6b) made in this material. This is somewhat unusual in a material with such a high hardness (an average of 900HV at 1000g load).

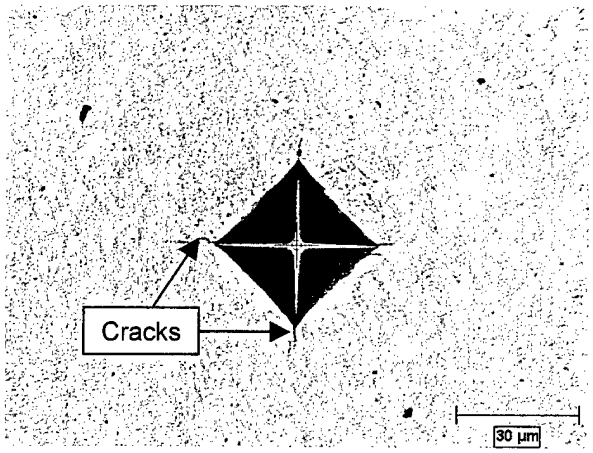

6a. Microhardness indentation under 1000g load in DAR27, Run 532.

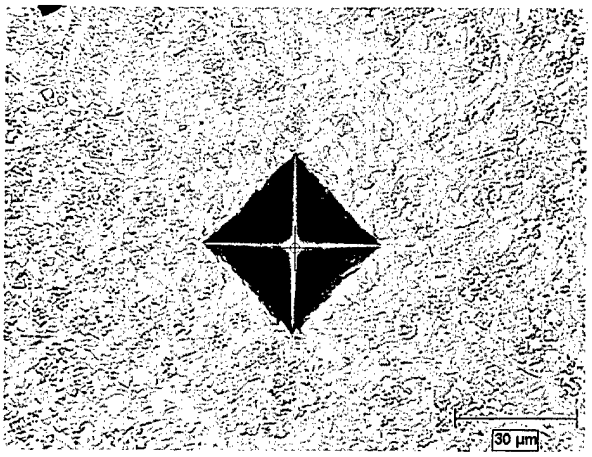

6b. Microhardness indentation under 1000g load in DAR35, Run 537.

Figure 6. Microhardness Indentations.

Table 5. Microindentation Hardness (Vickers) Results.

	Indent location	Top	Middle	Bottom	*Ave.*		Top	Middle	Bottom	*Ave.*
	Indent load	1000g	1000g	1000g			100g	100g	100g	
Run # (Alloy#)										
531 (DAR27)		1126	1010	1066	*1067*		1302	1302	1254	*1286*
532 (DAR27)		1096	1078	1072	*1082*		1231	1254	1327	*1271*
534 (DAR1A)		1159	1249	1199	*1202*		1465	1436	1465	*1455*
535 (DAR1A)		1072	974	1005	*1017*		1302	1187	1278	*1256*
536 (BMA)		902	964	969	*945*		1067	1105	1049	*1074*
537 (DAR35)		948	920	939	*937*		1005	1130	1180	*1138*

Porosity

Measurements of porosity were made of several of the runs. The results were as follows: Run 534 - 2.8%; Run 535 - 0.5%; Run 536 – 0.9%; and Run 537 – 1.08%.

Amorphous Phase Detection

Fracture surfaces of Runs 523 (DAR1A) and 527 (DAR27) are shown in Figures 7 and 8. Smooth and shiny surfaces, conchoidal patterns, and abrupt changes in fracture direction caused early speculation that the materials were amorphous. INEEL DSC analysis on samples from runs 523 (DAR1A) and 524 (DAR1A) did not show any evidence of glass, while DSC (Figure 9) and XRD (Figure 10) analyses at NSWC showed evidence of glass in runs 523 (DAR1A) and 524 (DAR1A). The XRD pattern (Figure 10a) from the run 523 sample has a minor peak, which indicates a predominately amorphous structure with some areas of crystalline phases and/or precipitates. The XRD pattern (Figure 10b) from the run 524 sample did not have any crystalline peaks, which indicates that the sample was amorphous. The different results at INEEL and NSWCCD are an indication that the proportions of amorphous and crystalline phases are varied throughout the spray formed microstructure of Runs 523 and 524. This is possible since cooling rates in the deposited material can vary with respect to time (i.e. averaging colder at the beginning of the run than at the end), as well as with respect to physical locations within the deposit (i.e. in the spray as a function of droplet diameter and radial position, or in the deposit as a function of local variations in the spray and deposit surface condition).

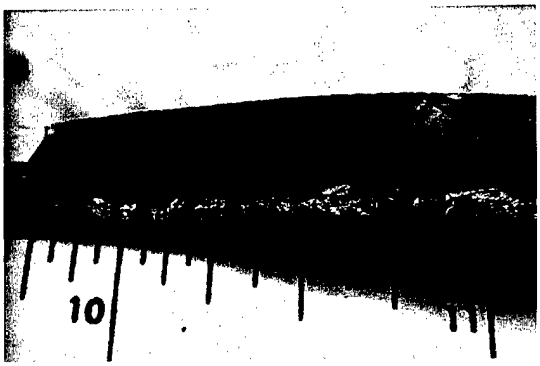

Figure 7. Run 523 fracture surface - DAR1A.

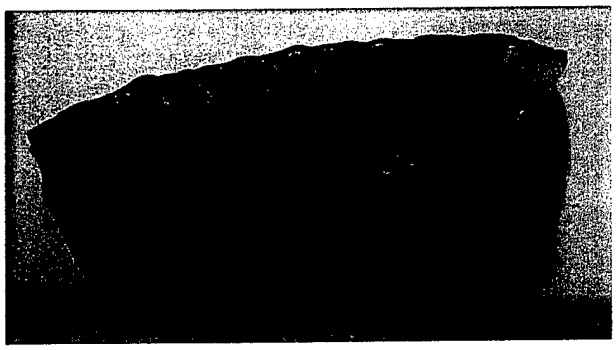

Figure 8. Run 527 fracture surface - DAR27.

DSC analysis was also performed on other spray forming runs: DAR 525, 526, 527, 532, 534, 536, and 537. The DSC pattern for these runs did not have crystallization peaks. DAR1A ingot, used as a melt charge for spray forming, also did not contain amorphous phases, while the DAR27 powder used as a melt charge did show a crystallization peak.

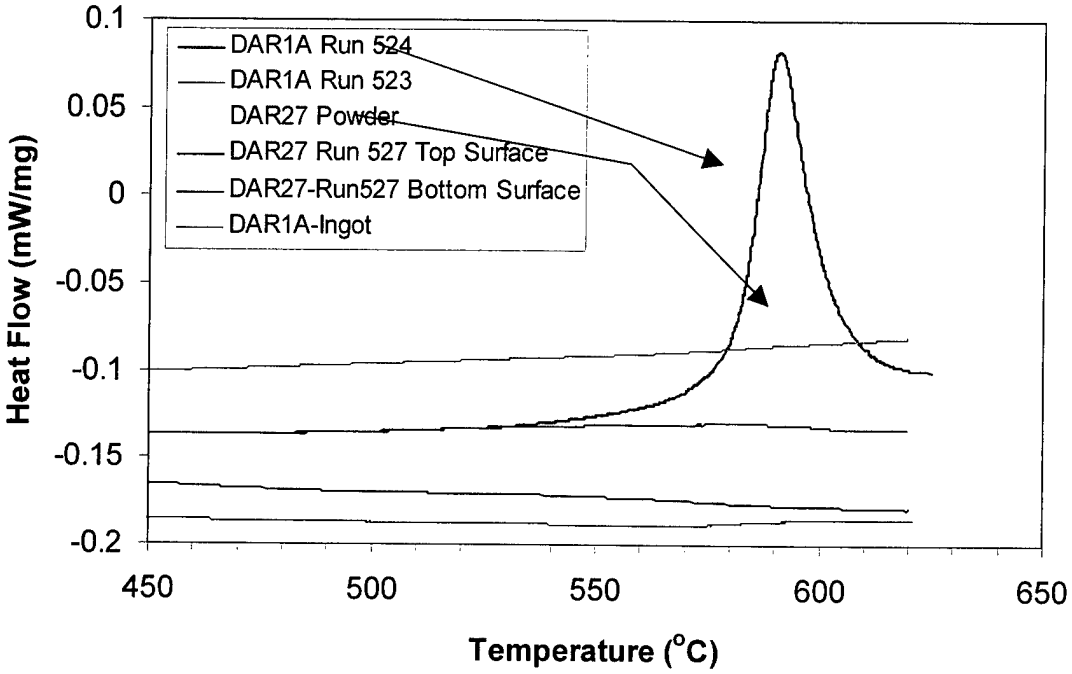

Figure 9. DSC plots of DAR1A and DAR27 alloys in spray formed, ingot, and powder forms.

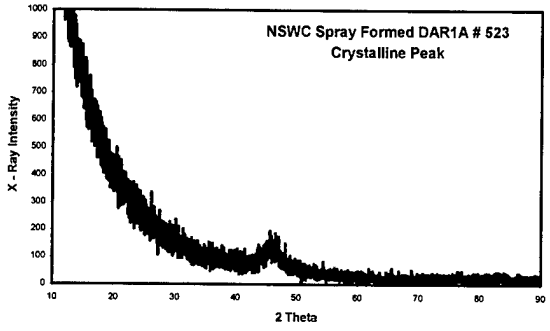

10a. DAR1A Run 523

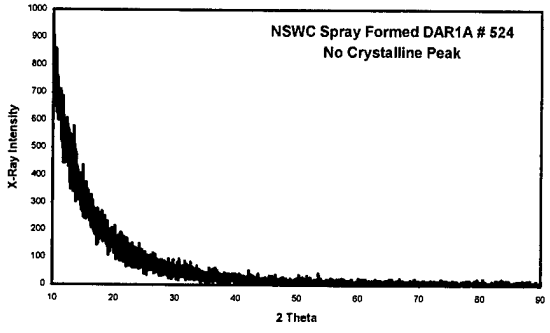

10b. DAR1A Run 524

Figure 10. XRD Pattern for Samples From Spray Forming Runs 523 and 524.

XRD patterns from runs 523, 524, 531, 536, and 537 showed areas in the runs that were partially amorphous. XRD patterns from samples taken from sections of the spray formed product that represent the beginning portion of a run (Figure 11) showed more amorphous material than in the sections towards the ends of the runs (Figure 12). The material at the end of the runs experiences the residual heat from the material that was sprayed before it, which could account for the greater fraction of crystalline material in the end sections of the runs. In addition, Figures 13 shows XRD patterns for Run 537, DAR35 in the as-sprayed condition and after a heat treatment of 700°C for 24 hours. There is a relatively minor change in the peak height and shape in the two patterns, which indicates that the remnant glassy material in Run 537, DAR35 is sluggish in transforming to the crystalline state. This suggests that this material is amenable to hot working without the loss of all of the glassy material to crystallization.

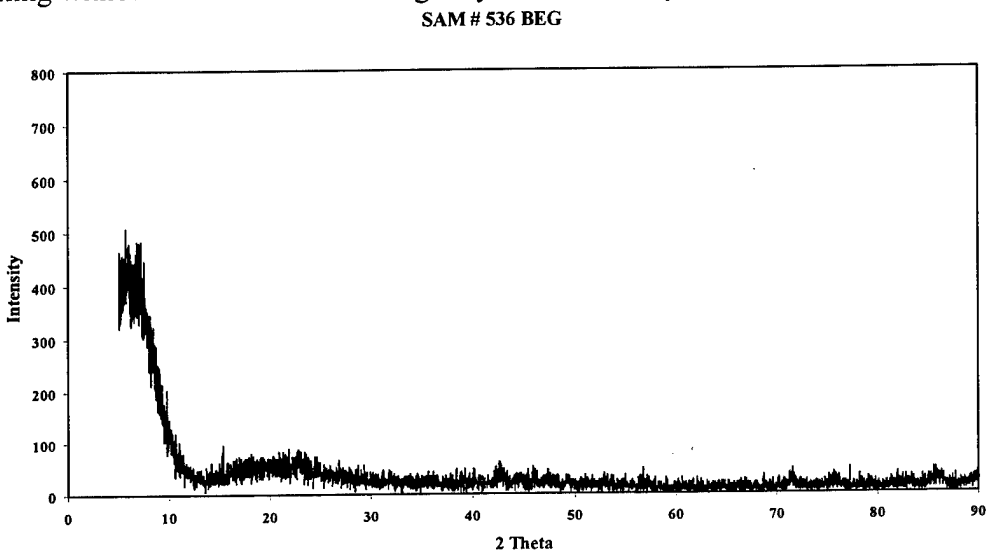

Figure 11. XRD of Material From Beginning Section of Run 536.

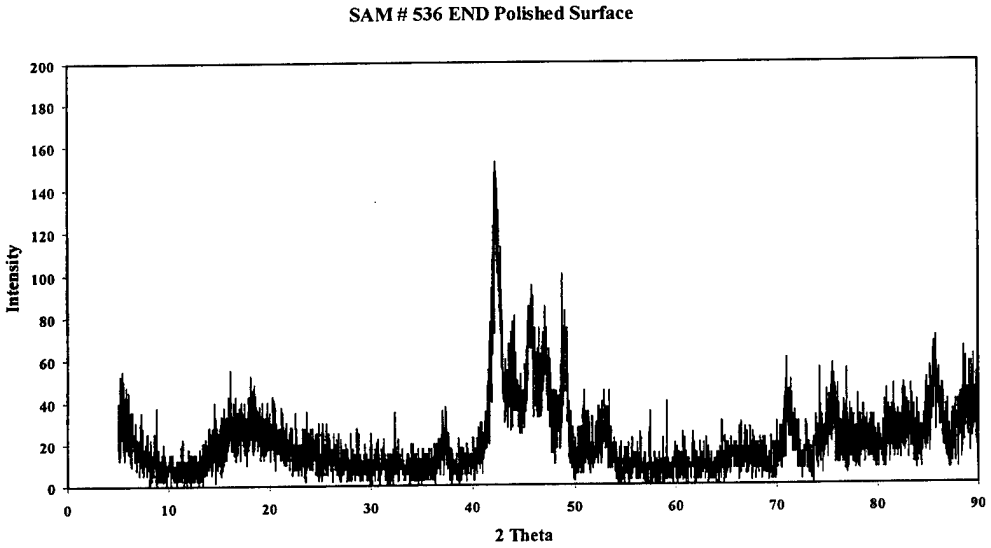

Figure 12. XRD of Material From End Section of Run 536.

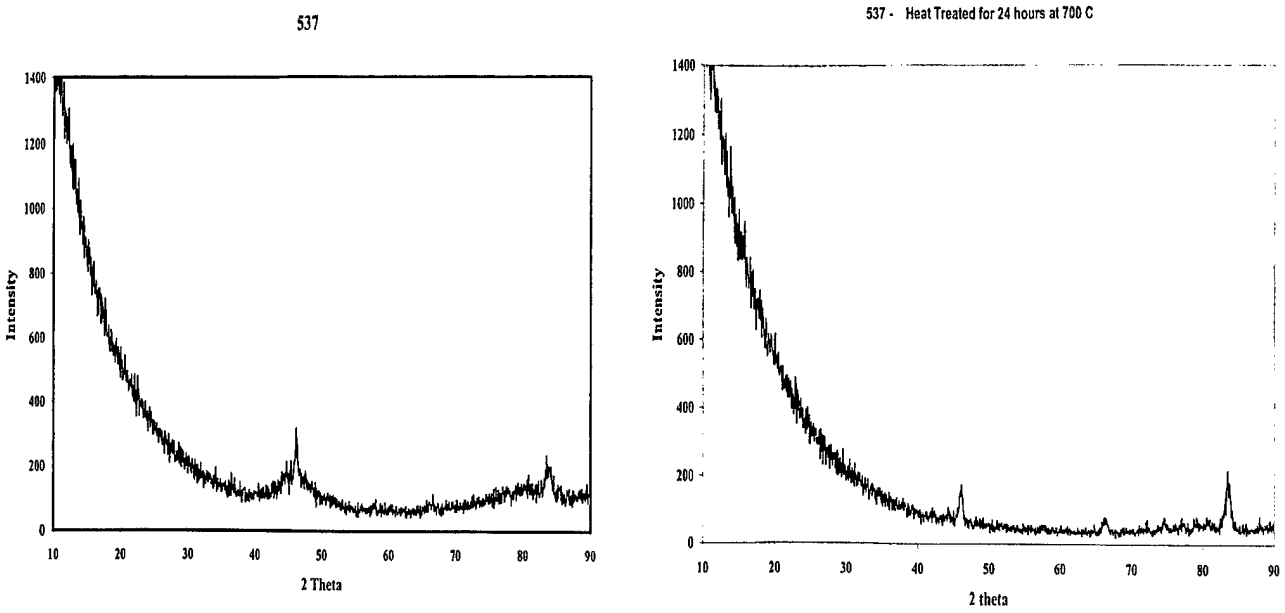

13a. XRD pattern for Run 537, DAR35 in the as-sprayed condition.

13b. XRD pattern for Run 537, DAR35 after heat treatment at 700°C for 24 hours.

Figure 13. XRD Patterns For Run 537, DAR35.

Macroscopy

As previously mentioned, after each of the spray forming runs, the material cracked (Figures 4 and 5). Most of the fracture surfaces had a very brittle appearance without signs of any plasticity (Figure 14). However, the fracture surface (Figures 15 and 16) from Run 537, DAR35 had some signs of plasticity. It indicates the potential for this material to exhibit plasticity in mechanical property tests. Additional spray forming runs with DAR35 are planned, and the material will be used for tensile strength tests.

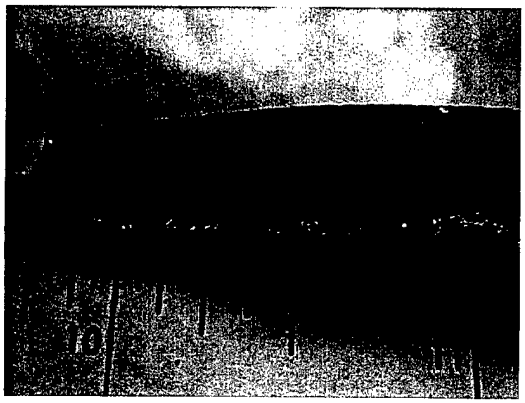

Figure 14. DAR 1A, Run 523, Mag. 2x.

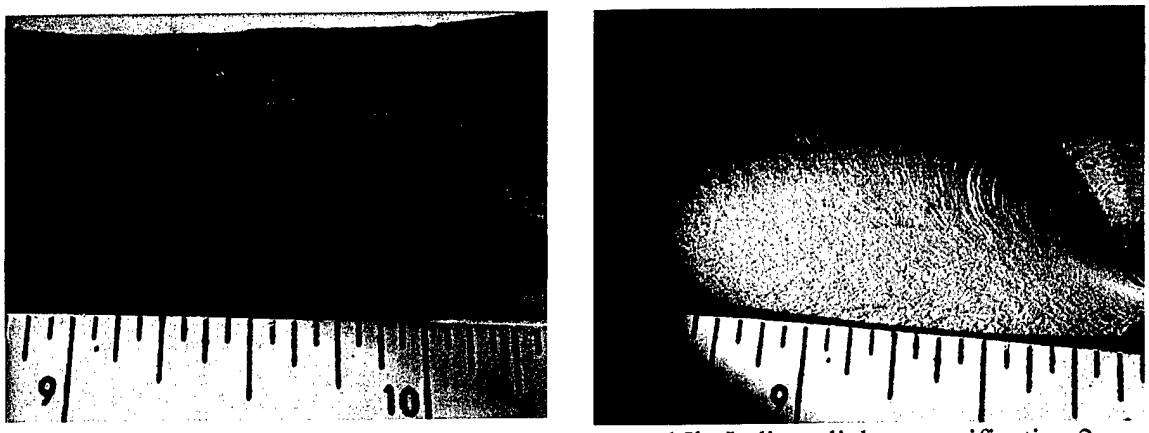

15a. Direct light, magnification 2x

15b. Indirect light, magnification 2x

Figure 15. Optical Macrographs of Fracture Surface on Piece of As-sprayed DAR35 From Run 537. (The inch is the unit of the rulers in the photos).

Figure 16. Scanning Electron Microscope, Secondary Electron Image of Fracture Surface on Piece of As-sprayed DAR35 From Run 537.

Microscopy

Samples from all of the spray formed runs were examined with the optical and scanning electron microscopes. The microstructures from Run 537, DAR35 was especially interesting. The optical microscope image is shown in Figure 17, and the scanning electron microscope, backscattered electron image (BSE) image is shown in Figure 18. In both figures three major phases are evident. For comparison purposes it should be noted that the white phase in the optical image appears light gray in the BSE image, the light gray phase in the optical image appears dark gray in the BSE image, and the dark gray phase in the optical image appears white in the BSE image. These phase equivalences between the optical and BSE images are also given in Table 6. An EDXA analysis on the SEM was used as an aid in identifying the elemental distribution in the phases. In Figure 17, the dark gray phase is a complex carbide of iron, molybdenum and chromium with some boron, silicon, and tungsten; the light gray phase is rich in iron and silicon with lesser amounts of the other elements; and the white phase is rich in iron, chromium, with lesser amounts of the other elements. Further work is needed to determine which of these phases is/are still amorphous.

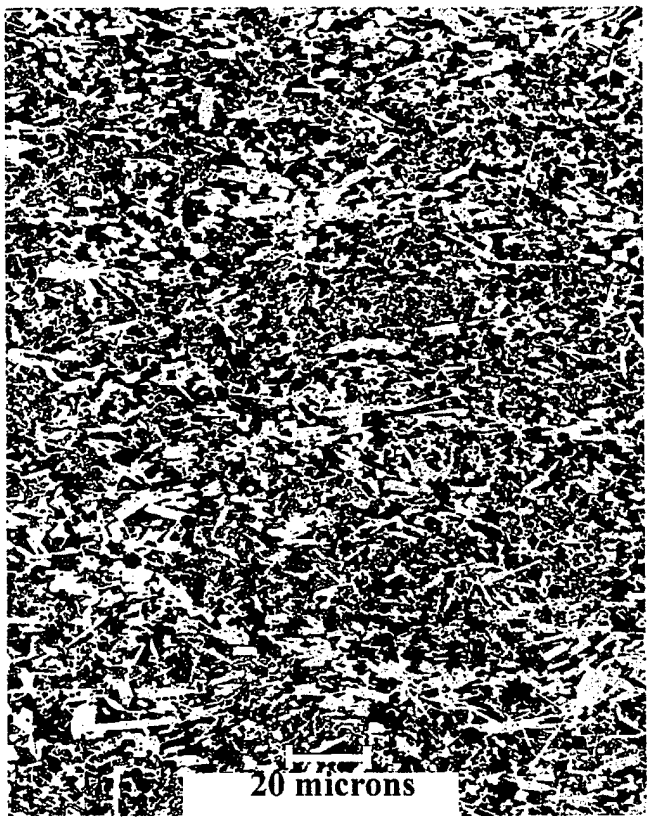

Figure 17. Optical Microscope Image of DAR35, Run 537, Etched.

Table 6. Phase Equivalences Between Optical (Figure 17) and BSE (Figure 18) Images of DAR35, Run 537.

Optical Image (Figure 15, etched)		BSE Image (Figure 16, unetched)
Dark gray, almost black	◄►	White
Gray	◄►	Dark Gray
White	◄►	Light Gray

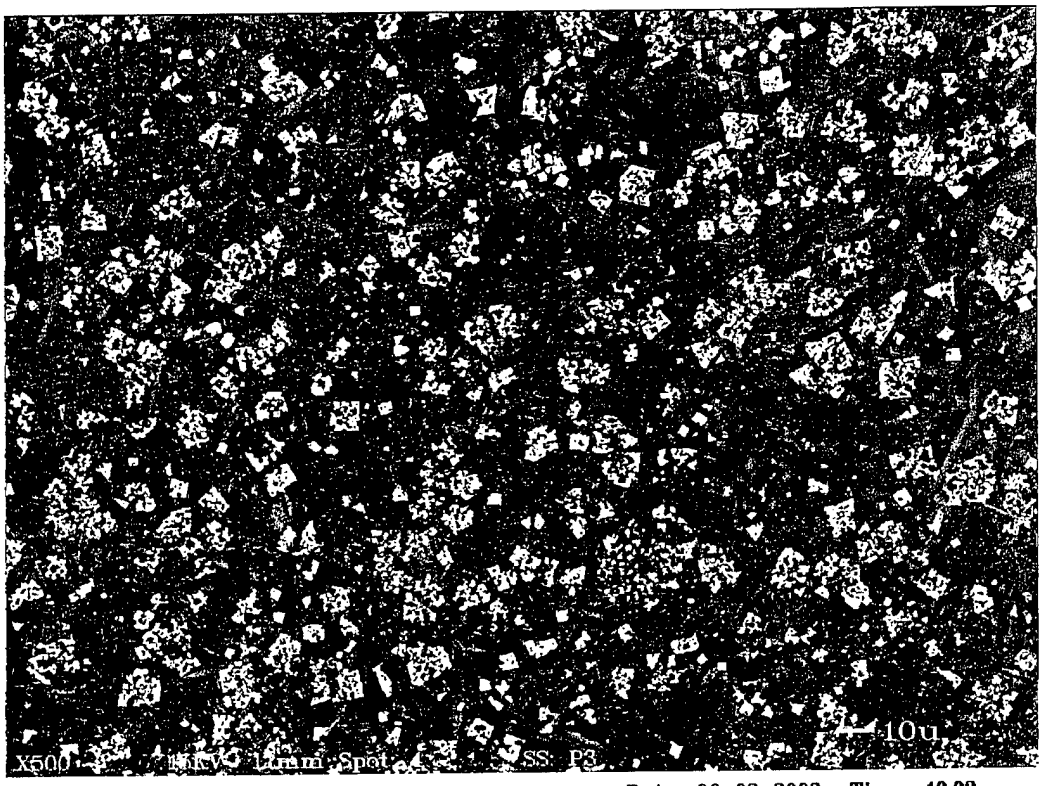

Title: DAR35 Run 537
Comment: 500x Area b BSE
Date: 06-03-2003 Time: 10:03
Filename: 35-B-BSE.TIF

Note: Black spots on image are pores in the microstructure.

Figure 18. Scanning Electron Microscope, Backscattered Electron Image, DAR35, Run 537, Unetched.

The composition of DAR35 is a higher silicon version of DAR27. DAR35 has 5 at. % silicon versus 1 at. % for DAR27 with the other alloying additions held the same. This difference in silicon created a marked difference in the microstructure of the two alloys. Optical and scanning electron microscope images for DAR27, Run 532 are shown in Figures 19 and 20. In comparing the BSE images (Figures 18 and 20), it appears that DAR35 has more carbides (the white phase) and more of a dark gray phase. EDXA of the phases in Figures 18 and 20 showed a composition difference in the dark gray phases in the images. Specifically, the dark gray phase in the BSE image of DAR35 (Figure 19) is silicon rich; the dark gray phase in the BSE image of DAR27 (Figure 20) is not silicon rich. There is also a morphological difference in the light gray phase in each of the images. In DAR35 the light gray phase is more needle-like.

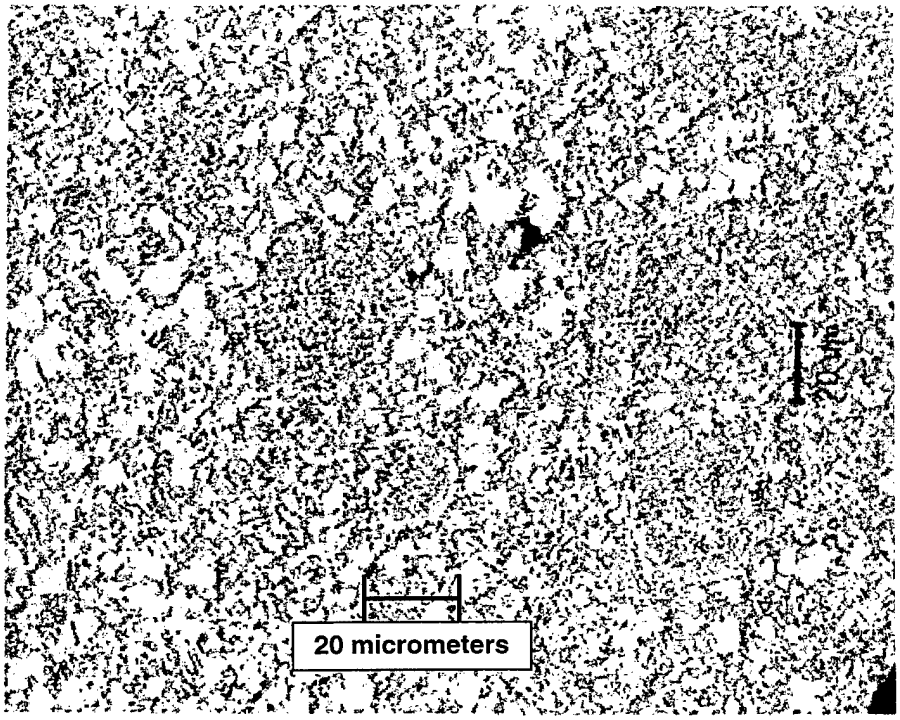

Figure 19. Optical microscope image of DAR27, Run 532, etched.

Title: DAR35 Run 532
Comment: 500x Area a–BSE
Date: 06–04–2003 Time: 14:56
Filename: 532A–BSE.TIF

Note: Black spots on image are pores in the microstructure.

Figure 20. Scanning Electron Microscope, Backscattered Electron Image, DAR27, Run 532, Unetched.

Corrosion Results

After exposure for 24 cycles (1000 total hours) in the salt fog chamber, all of the samples showed extensive corrosion in the form of rust. Since all of the samples were partially de-vitrified and contained ferrite, the rust was to be expected. The extent of the rusting was similar to that for an unpainted hull steel, such as HSLA 80. Before and after photographs of the samples of DAR1A and DAR27 are given in Figures 21, and 22, respectively. A photograph of the sample of DAR35 after 5 cycles is shown in Figure 23. Also shown in Figure 23 are control samples of HSLA 80 and Inconel 625.

The University of Virginia has two compositions that they believe will be more corrosion resistant than some of the DAR alloys produced by INEEL. One composition is designated 02-428 and consists of Fe51Mn10Mo14Cr4C15B6; the other is designated 02-234 and consists of Fe53Mn10Mo12Cr4P7C7B7. As this material becomes available to us, we intend to spray metal form samples for corrosion tests.

These results leave unanswered the question as to whether the iron-based amorphous metals would be corrosion resistant if fully amorphous. To answer this question, Prof. Joe Poon at the University of Virginia has produced 4 mm diameter pins samples of an iron-based SAM (Fe51Mn10Cr4Mo14C15B6), in three conditions – fully amorphous, partially devitrified, and fully devitrified. These samples are currently being exposed in our salt fog test.

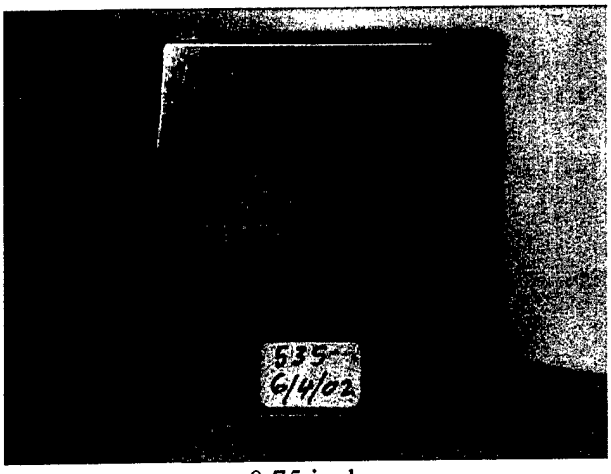

0.75 inch

21a. Salt fog sample of DAR1A, Run 535 before exposure.

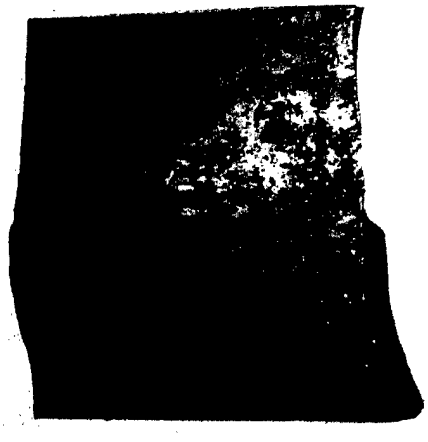

0.75 inch

21b. Salt fog sample of DAR 1A, Run 535 after 7 cycles.

Figure 21. Photographs of Salt Fog Corrosion Samples of DAR1A, Run 535 Before and After Exposure.

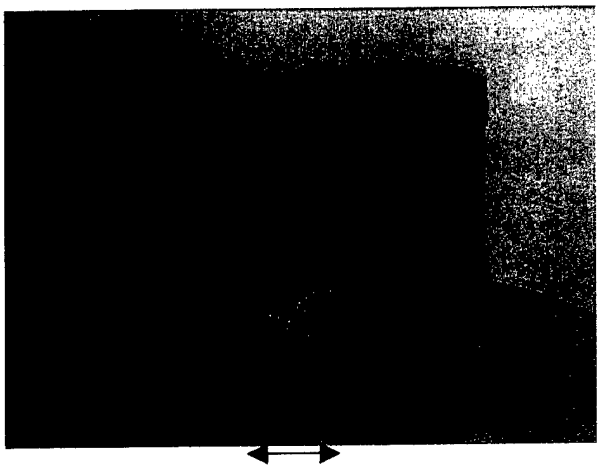

0.75 inch

22a. Salt fog sample of DAR27, Run 532 before exposure.

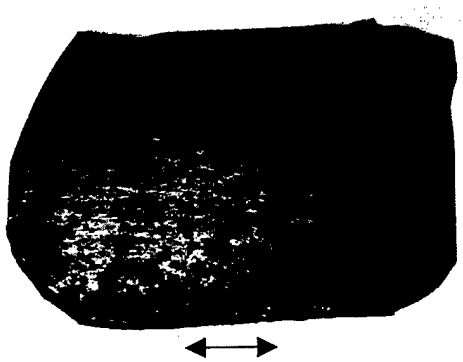

0.75 inch

22b. Salt fog sample of DAR27, Run 532 after 7 cycles.

Figure 22. Photographs of Salt Fog Corrosion Samples of DAR27, Run 532 Before and After Exposure.

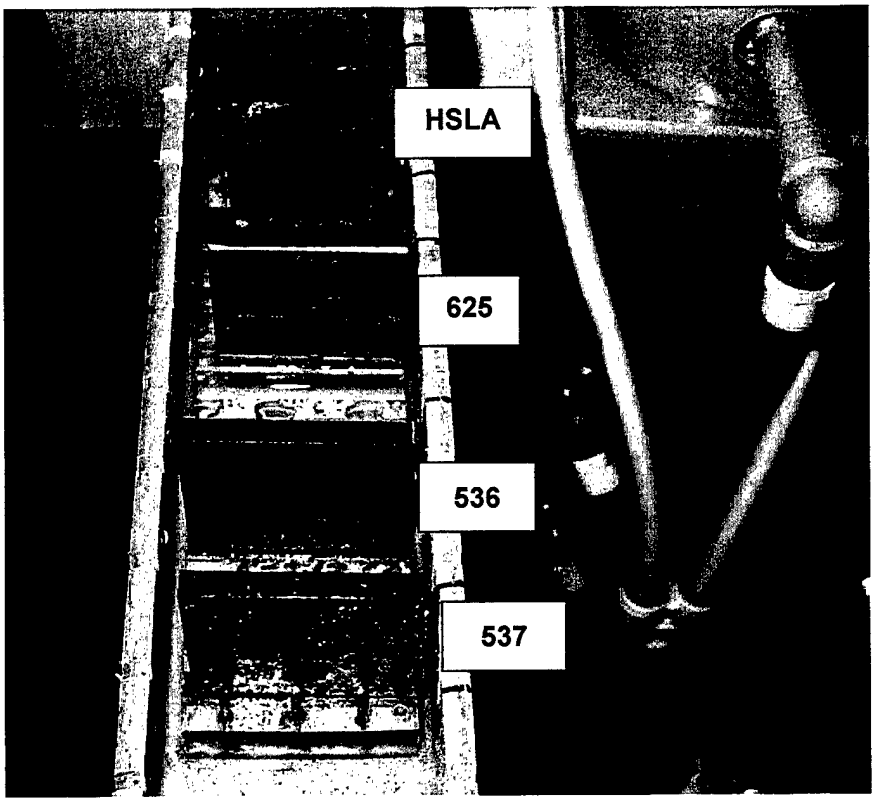

Figure 23. Photographs of Salt Fog Corrosion Samples of DAR35 (Run 537), DAR1A (Run 536), HSLA 80 and Inconel 625 after 5 cycles.

Wear Test Results

The complete wear test report from the University of Colorado is given in Appendix A. It includes data on the spray metal formed samples as well as coated iron based SAMs. The data on the coatings will be the subject of a separate report. The wear results are summarized in Table 7 for the spray metal formed samples.

Table 7. Comparison of Specimen Wear Rates.

Sample Name	Volume Loss Segment 1 (mm^3)	Lineal Abrasion (m)	Normal Load (N)	Normalized Volume Loss ($mm^3/m/N$)
DAR27, Run 531 (side 1)	2.3	718	130	0.0000249
DAR27, Run 531 (side 2)	2.4	718	130	0.0000257
DAR35, Run 537 (side 1)	2.7	718	130	0.0000289
DAR35, Run 537 (side2)	3.0	718	130	0.0000321
BMA1, Run 536 (side 1)	21.9	718	130	0.0002346
BMA1, Run 536 (side 2)	24.5	718	130	0.0002624
HSLA 100 (side1)	44.7	718	130	0.0004788
HSLA 100 (side 2)	48.3	718	130	0.0005173
D2 Tool Steel*	36.4	4309	130	0.0000650

*Procedure A. All other samples procedure E in Appendix 1

The results above suggest that specimen DAR27, Run 531 is the most wear resistant. The wear results for DAR35, Run 537 are nearly equivalent to DAR27. All of the DAR samples were more wear resistant than the tool steel sample; the BMA samples were less wear resistant. The conventional hull plate alloy, HSLA100, is the least wear resistant of the samples tested.

Summary

Metal spray forming has been used to produce iron-based products with partially amorphous microstructures. This was possible through the use of low critical cooling rate alloys and rapid solidification in the metal spray. The products of metal spray forming were either tubular or flat deposits ranging in thickness of ½" to 1¼". Amorphous and crystalline content in these deposits varied according to the position within the deposits as well as with the processing parameters. Severe, spontaneous cracking occurred in all spray formed deposits during the slow cooling period that follows spray deposition. It is hypothesized that this is a result of the combination of coefficient of thermal expansion differences with the substrate and the brittle nature of the deposit material. The use of a pre-heated substrate is being investigated to minimize or eliminate this cracking. The spray formed deposits had high hardness (900 to 1200 HV), low porosity, (0.5 to 3%), and better wear resistance than a conventional hull steel and a tool steel. In a standardized salt fog chamber test, the spray formed alloys were found to corrode like a conventional hull steel. This is a probably a result of the partially devitrified nature of the spray formed material.

This page intentionally left blank

References

1. Hays, C. C., C. P. Kim, and W. L. Johnson, "Microstructure Controlled Shear Band Pattern Formation and Enhanced Plasticity of Bulk Metallic Glasses Containing *in situ* formed Ductile Phase Dendrite Dispersions", Phy. Rev. L., Vol. 84, No. 13, 27 Mar 2000.

2. Inoue, A., "Bulk Amorphous Alloys With Soft and Hard Magnetic Properties", Mat. Sci. and Eng., A226-228, (1997), pp. 357-363.

3. www.webref.org

This page intentionally left blank

Appendix A

Abrasive Wear Tests of Various Coupons

Paul Shoemaker, Michael Gardner, and Paul Wilbur
PI: John Williams
Department of Mechanical Engineering
Colorado State University
during
March 2003

For
Dr. Leslie Kohler and Dr. Louis Aprigliano
Naval Surface Warfare Center
Carderock Division

Apparatus and Procedures

Abrasive wear tests of four surface-coated specimens and four solid specimens provided by NSWC-Carderock were conducted per ASTM G65-00 (Standard Test Method for Measuring Abrasion Using the Dry Sand/Rubber Wheel Apparatus). The tests were performed using an apparatus like the one shown schematically in Fig. 1. Wear results were obtained using Procedure E for all NSWC specimens and the calibration procedure (Procedure A) for the D2 tool steel specimen. The four surface-coated specimens were only tested on the side with the surface coating while the four solid specimens were tested on both sides, totaling twelve abrasive wear tests. The solid specimens were labeled differently on each side in order to establish correspondence between a test and a wear scar. Abrasive wear tests were initiated by first cleaning the specimen with acetone. The specimen dimensions were measured along with an initial mass. All mass measurements are accurate to 0.0001 grams. The specimen was mounted in the specimen holder, and a uniform sand flow curtain was established between the specimen and the rubber wheel at a sand flow rate of between 300 and 400 grams per minute. The rubber wheel was turned on and rotated at 250 rpm. Once the sand flow curtain was uniform, a 130 N normal (i.e. radial) force was applied between the specimen and the rubber wheel. Wheel revolutions were counted from the time that the rotating rubber wheel and specimen came into contact. The specimen was separated from the rubber wheel after the completion of the required

number of revolutions, and the elapsed time was recorded. Once the specimen was removed from the specimen holder, a depth profile of the wear scar was taken perpendicular to the direction of relative motion at approximately the scar midpoint. The specimen mass was then measured again at the end of the test, and a mass loss was calculated. The mass loss of all specimens was converted to a volume loss using the specimen density data provided by NSWC-Carderock. In addition, the density of the solid specimens 536BMA1, 531DAR27, 537DAR35, and HSLA100 were calculated using the measured specimen dimensions and the original specimen mass.

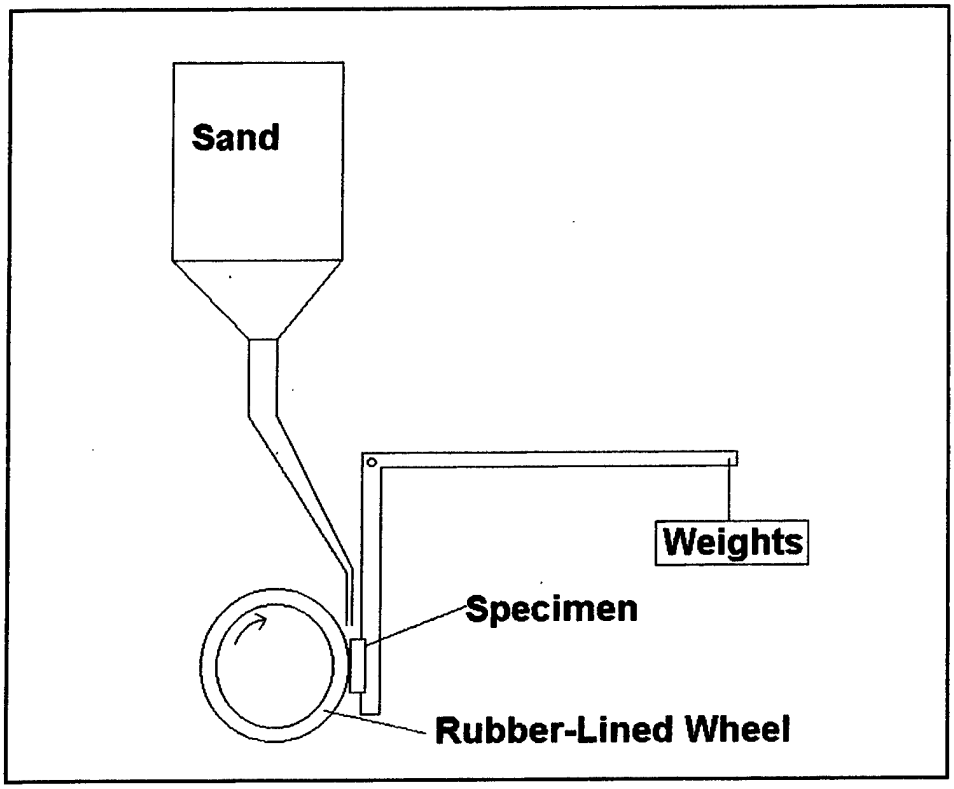

Figure 1. ASTM G-65 Test Setup Schematic

Wear tests were conducted in two, 1000-revolution segments using the procedure described in the preceding paragraph for each segment. Special care was taken to remove the specimen after the first segment and then reinstall it for the second segment so that the wear scar was aligned properly with the rubber-lined wheel. Performing a second 1000-revolution segment over an existing wear scar is not standard testing procedure according to ASTM G65-

00. It was performed in these cases to check if the surface-coated specimens coating had been penetrated. The two, 1000-revolution segments were performed on all specimens, including the solid specimens, in order to provide consistency between results. The second segment will not be used to rank the specimen wear performance in this report.

Calibration of the dry sand/rubber wheel testing apparatus at the Engineering Research Center at Colorado State University was performed using a D2 tool steel specimen. The ASTM G65-00 standard specifies a volume loss of 35.6 ± 5.2 mm^3 for 6000 revolutions (ASTM G65-00 Procedure A). The D2 tool steel specimen wear test was conducted in three, 2000-revolution segments using the procedure described above. Special care was taken to remove the specimen after the first and second segments and then reinstall it for the second and third segments, respectively, so that the wear scar was aligned properly with the rubber-lined wheel. The results for the three test segments were a total D2 tool steel specimen volume loss of 36.4 mm^3, an error of ~2%. The calibration of the CSU testing apparatus falls within the limits specified by ASTM G65-00.

Results

Figure 2 shows a typical micrograph of a wear scar. The micrograph was taken after both test segments were performed, for a total of 2000 revolutions. Figure 3 shows the corresponding depth profile measured perpendicular to the direction of relative motion at approximately the midpoint. Depth profiles of the wear scar after both test segments are shown in Figure 3.

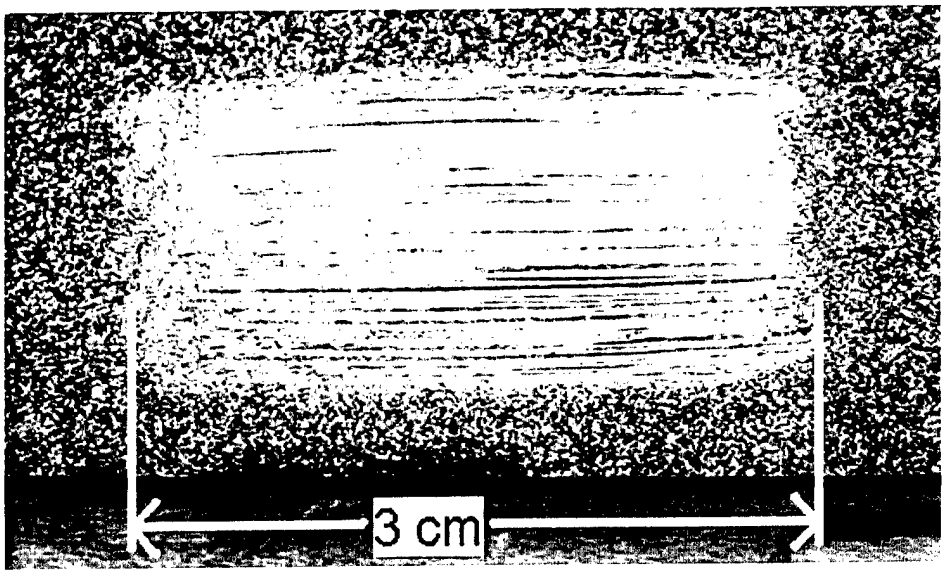

Figure 2. Typical (NWA-35-AS) Wear Scar

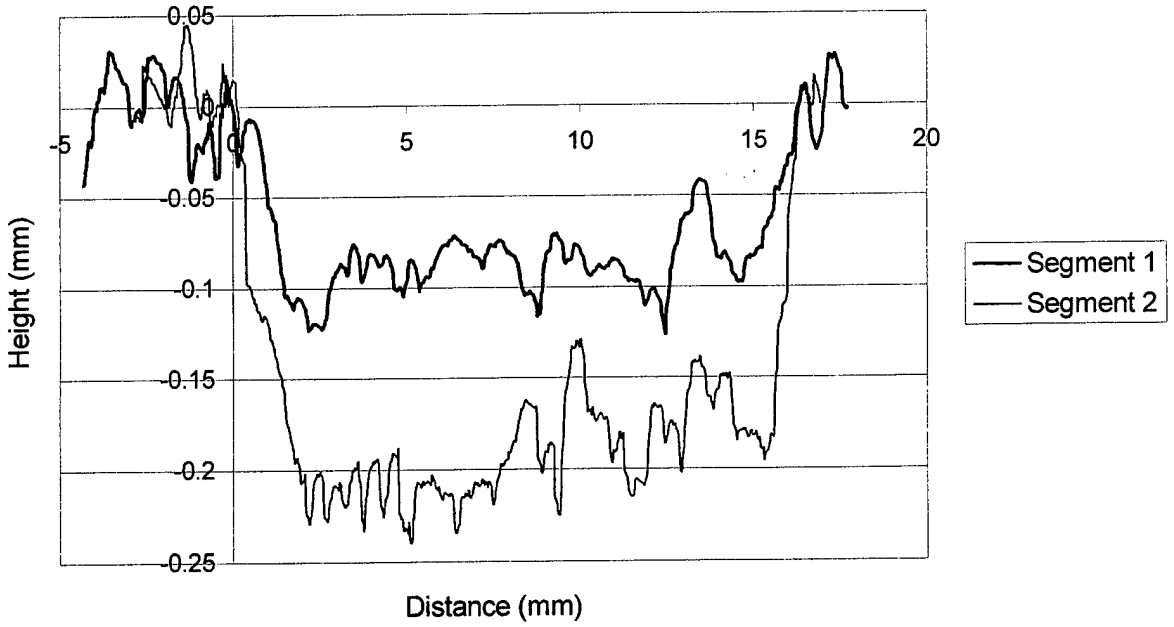

Figure 3. Typical Wear Profiles

A data sheet giving test results for a typical specimen is shown in Table 1. Similar data sheets containing results obtained from all specimens in the batch are included in Appendix A of this report. In each case, the first line of the data sheet shows the test segment number, the specimen identification (NWA-35-AS for Table 1), and the test date. The NSWC-Carderock-provided density of the coating is given on the next line. It is noted that the density for specimen

536BMA1 was provided by measurements made by Dr. Leslie Kohler and not by the specimen manufacturer. If the specimen was a solid one the next line shows the measured density, and it is marked N/A if it was a surface-coated specimen.

Table 1. Typical (NWA-35-AS) Data Sheet

Segment 1 was performed on Sample NWA-35-AS on 3/9/03

7460 kg/m^3	Provided Density
N/A kg/m^3	Measured Density
250 RPM	
4 Minutes	
1000 Revolutions (ASTM G65-00 Procedure E)	

The following masses are in grams

Initial Mass (g):	69.5608	69.5605	69.5604	69.5605	69.5605
	69.5568	69.5569	69.5569	69.5568	69.5567
Final Mass (g):	69.4481	69.4481	69.4481	69.4482	69.4481
	69.4476	69.4476	69.4474	69.4476	69.4476

Average Initial Mass (g): 69.5587 **St. Dev. (g):** 0.0019
Average Final Mass (g): 69.4478 **St. Dev. (g):** 0.0003

0.1106 gram	Mass Loss
14.8 mm^3	**Volume Loss using provided density**

The next three lines show the calculated RPM rate, the recorded time, and the recorded wear test revolutions, respectively. The corresponding ASTM G65-00 procedure is identified next to the number of revolutions. The next rows of data are the initial masses measured 5 times in one day and then 5 times again more than 24 hours later. If the mass results were inconsistent, the mass was measured again more than 24 hours after the last measurement until consistent results were obtained. This was done to assure that acetone that might have accumulated during block cleaning was not evaporating and affecting the measurements. After each wear test, the final mass was recorded in a similar way involving measurements made before and after a 24-hour interval. Mean masses of two sets of these measurements—one made before the abrasive wear test and one made after it—are shown along with a standard deviation for each set. These

data were used to compute a wear-test-induced mass loss. The volume loss given was obtained by dividing this mass loss by the provided density.

The final wear results for all of the specimens are reported in Table 2. In order to obtain consistent wear test results, only the first 1000 revolution segment is reported when ranking the specimens. The second 1000 revolution segment was performed to provide a check that the surface-coated specimens coating had not been penetrated. Data for the second segment can be found in Appendix A for all specimens. The lineal abrasion distance reported for each specimen is equal to the circumference of the rubber-lined wheel multiplied by the number of revolutions. All NSWC specimens had a lineal abrasion distanced calculated for a 1000 revolution wear test (ASTM G65-00 Procedure E), while the D2 tool steel specimen calculated the lineal abrasion based on a 6000 revolution wear test (ASTM G65-00 Procedure A). The normal load of 130 N for all specimens is also reported. Finally, a normalized volume loss, which is the measured volume loss divided by both the lineal abrasion distance and by the normal load, is shown. The volume results listed are based on density data provided by Carderock and do not rely on the measured density data. The specimens are ranked in order of normalized volume loss, with the smallest normalized volume loss at the top.

In addition, the results for the abrasive wear tests on seven surface-coated specimens reported previously after September 2002 tests are given in Table 3. These data are included because the original September 2002 report calculated lineal abrasion and therefore normalized volume loss based on both test segments for a total of 2000 revolutions. Here, the September 2002 specimen data are reported in Table 3 in the same manner as the current specimen data in Table 2. The data sheets for both test segments for the September 2002 specimens are included.

Table 2. Comparison of Specimen Wear Rates

Sample Name	Volume Loss Segment 1 (mm^3)	Lineal Abrasion (m)	Normal Load (N)	**Normalized Volume Loss ($mm^3/m/N$)**
531DAR27	2.3	718	130	0.0000249
531	2.4	718	130	0.0000257
537	2.7	718	130	0.0000289
537DAR35	3.0	718	130	0.0000321
D2 Tool Steel*	36.4	4309	130	0.0000650
NHV-NANO-AS	6.0	718	130	0.0000643
NWA-35-AS	14.8	718	130	0.0001585
536BMA1	21.9	718	130	0.0002346
536	24.5	718	130	0.0002624
NWA-27-AS	25.1	718	130	0.0002688
NHV-35-AS	38.3	718	130	0.0004102
HSLA100	44.7	718	130	0.0004788
HSLA100b	48.3	718	130	0.0005173

* Procedure A. All other samples Procedure E.

Table 3. Comparison of September 2002 Specimen Wear Rates

Sample Name	Volume Loss Segment 1 (mm^3)	Lineal Abrasion (m)	Normal Load (N)	**Normalized Volume Loss ($mm^3/m/N$)**
IHV-27-700	7.8	718	130	**0.0000831**
NHV NANO-27-AS	8.6	718	130	**0.0000926**
IHV-27-AS	16.0	718	130	**0.0001716**
NHV-27-AS	18.4	718	130	**0.0001968**
IWA-27-700	18.6	718	130	**0.0001994**
NWA-27-AS	23.9	718	130	**0.0002559**
IWA-27-AS	28.0	718	130	**0.0003001**

The final wear profile of each specimen was also used to calculate the cross-sectional area of the wear track. The cross-sectional area was converted to a volume loss by assuming the wear track had a maximum cross sectional area at the wear profile location, which was approximately the middle of the wear scar, and that this area decreased linearly to zero at both ends. Table 4 shows the total volume loss after 2000 revolutions computed by both methods, and the percent error of the profile method. The relatively large errors shown in Table 4 indicate

that the wear profile technique should not be used for calculating volume loss. However, the wear profile data are useful in determining if the coatings were worn through.

Table 4. Volume Loss Method Comparison

Sample Name	Total Volume Loss (mm^3) over 2000 revolutions		Percent Error
	Mass Method	Profile Method	
531	3.4	3.5	3
531DAR27	3.6	1.5	59
537	4.1	3.2	22
537DAR35	5.1	1.9	63
NHV-NANO-AS	9.0	8.8	2
NWA-35-AS	24.4	32.1	32
NWA-27-AS	40.4	27.8	31
536BMA1	42.2	28.3	33
536	43.8	40.5	8
NHV-35-AS	113.2	139.1	23
HSLA100b	95.5	63.9	33
HSLA100	98.1	101.0	3

The ASTM G65-00 abrasive wear test has several error sources associated with it. One possible source of error in the experimental results is that due to mass measurement error. In most cases, the specimen mass was only determined twice with an interval of at least 24 hours between each set of five measurements. There were a few cases in which results obtained on the two days were inconsistent. In these cases, measurements were made a third or even fourth time to get consistent results. It is believed that differences between the mass measurements were due to acetone evaporation effects or debris on the weighing pan. Only two sets of mass measurements made more than 24 hours apart were used to obtain a mean final mass. In most cases, the mean mass loss was at least two orders of magnitude greater than the standard deviation of the mass measurement, which suggests that the mass measurement errors are small.

Another possible source of error is related to the uniformity of the wear scar. In all cases, a modest difference in the length of the wear scar and the depth of the wear scar at the two edges was observed. This error was traced to non-uniform sand flow from the nozzle and minor imperfections of the wheel itself. This caused one side of the specimen to contact the wheel slightly before the other as the two surfaces were loaded together statically. In some instances,

the unevenness was compounded by the fact that not all of the samples were perfectly flat, and shims were used to minimize this effect. A calibrated revolution counter and dead weight loading scheme assured that errors due to these factors were negligible. Rubber wear on the wheel surface leading to a change in wheel circumference was also negligible.

Discussion

The second segment of each test generally wore only about 60 percent as much as the first segment. D2 tool steel exhibited this characteristic wear pattern as well, with the first 2000-revolution segment wearing twice as much as the following two segments. It was decided to use Procedure E (1000 revolutions) for the Carderock-provided samples to avoid wearing through the 0.4 mm minimum thickness of the coated samples.

It was determined that the second wear test segment on specimen NHV-35-AS wore through the specimen coating and into the base coupon metal. Figure 4 shows the NHV-35-AS wear scar with the exposed base metal marked in white. Figure 5 shows the NHV-35-AS wear profile after each of the two test segments. The second wear profile segment shows a maximum wear scar depth of 0.9 mm which is much greater than the minimum coating thickness of 0.4 mm. As a consequence, NHV-35-AS had a much higher volume loss for the second segment of the test than for the first.

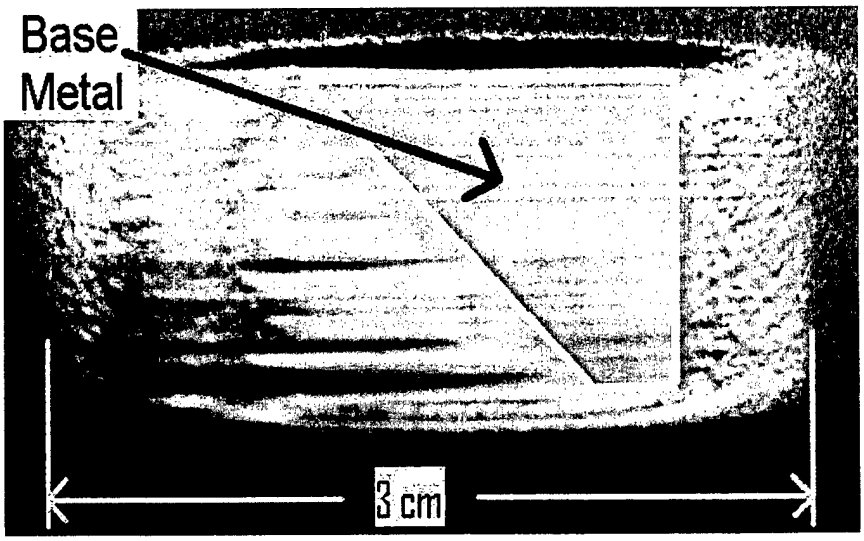

Figure 4. NHV-35-AS Wear Scar

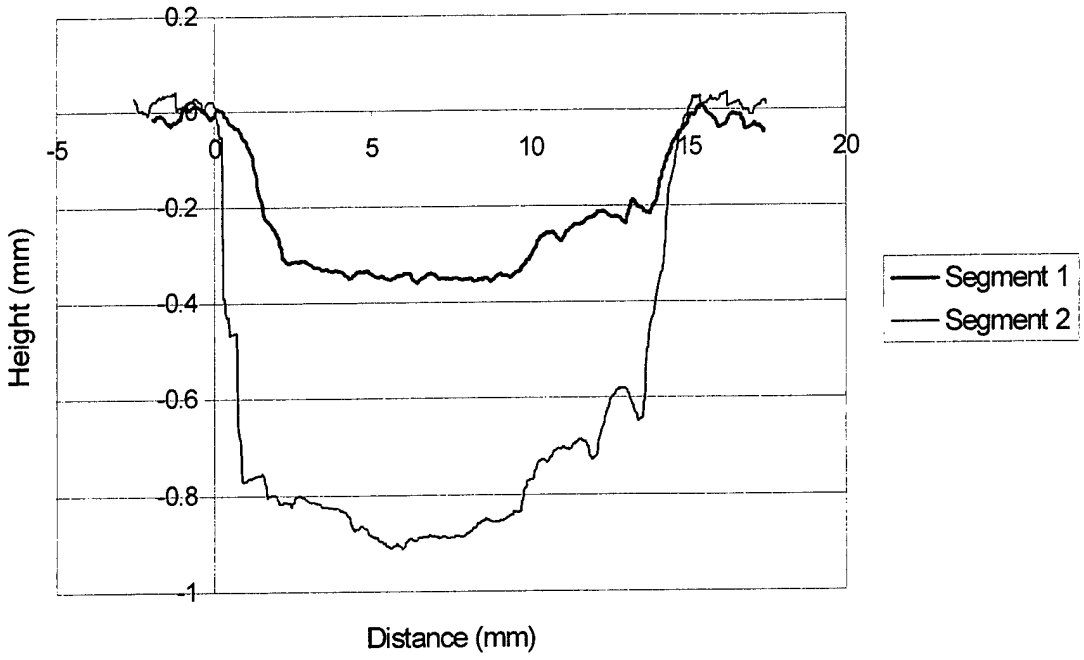

Figure 5. NHV-35-AS Separate Wear Profiles

Tribological test results can vary substantially as the many parameters of the test are varied, therefore the results of Table 2 should be considered only for purposes of gross screening of the various surface-coated specimens and solid specimens. In actual applications, the relative performance of the various specimens could be different. Thus, screening tests suggest that specimen 531DAR27 is the most wear resistant and specimen HSLA100b is the least wear resistant of the samples provided.

Distribution

DoD - CONUS	Copies
CHIEF OF NAVAL RESEARCH ATTN 332 (CHRISTODOULOU) BALLSTON CENTRE TOWER ONE 800 NORTH QUINCY ST ARLINGTON VA 22217-5660	1
COMMANDER NAVAL SEA SYSTEM COMMAND ATTN SEA 05M (KAZNOFF) 1333 ISAAC HULL AVE SE STOP 5130 WASHINGTON NAVY YARD DC 20376-5130	1
COMMANDER NAVAL SEA SYSTEMS COMMAND ATTN SEA 05M2 (NULL) 1333 ISAAC HULL AVE SE STOP 5132 WASHINGTON NAVY YARD DC 20376-5132	1
DEFENSE ADVANCED RESEARCH PROJECTS AGENCY DEFENSE SCIENCE OFFICE ATTN DR L CHRISTODOULOU 3701 NORTH FAIRFAX DR ARLINGTON VA 22203-1714	1
DEFENSE TECH INFO CTR 8725 JOHN KINGMAN ROAD SUITE 0944 FORT BELVOIR VA 22060-6218	1

INTERNAL		Copies
CODE 0115		1
CODE 60		1
CODE 61	(DENALE)	1
CODE 612	(APRIGLIANO)	6
ODE 612	(KOHLER)	2
CODE 613	(HAYS)	1
CODE 614		1
CODE 615	(DELOACH)	1
CODE 3442	(TIC)	1

This page intentionally left blank

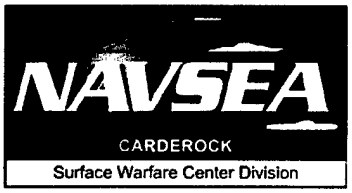
NAVSEA
CARDEROCK
Surface Warfare Center Division